ACCOUNTS
of chemical research

Article

Clay, Water, and Salt: Controls on the Permeability of Fine-Grained Sedimentary Rocks

Published as part of the Accounts of Chemical Research special issue "Chemistry of Geologic Carbon Storage".

Ian C. Bourg*,†[ID] and Jonathan B. Ajo-Franklin§

†Princeton University, Department of Civil and Environmental Engineering (CEE) and Princeton Environmental Institute (PEI), Princeton New Jersey 08544, United States
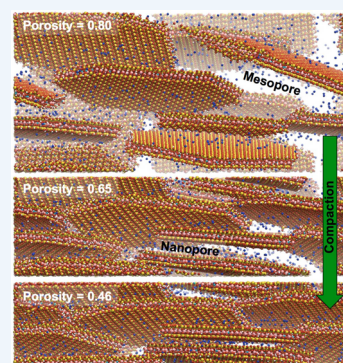
§Lawrence Berkeley National Laboratory, Energy Geoscience Division, Berkeley California 94720, United States

CONSPECTUS: The ability to predict the permeability of fine-grained soils, sediments, and sedimentary rocks is a fundamental challenge in the geosciences with potentially transformative implications in subsurface hydrology. In particular, fine-grained sedimentary rocks (shale, mudstone) constitute about two-thirds of the sedimentary rock mass and play important roles in three energy technologies: petroleum geology, geologic carbon sequestration, and radioactive waste management. The problem is a challenging one that requires understanding the properties of complex natural porous media on several length scales.

One inherent length scale, referred to hereafter as the *mesoscale*, is associated with the assemblages of large grains of quartz, feldspar, and carbonates over distances of tens of micrometers. Its importance is highlighted by the existence of a threshold in the core scale mechanical properties and regional scale energy uses of shale formations at a clay content $X_{clay} \approx 1/3$, as predicted by an ideal packing model where a fine-grained clay matrix fills the gaps between the larger grains. A second important length scale, referred to hereafter as the *nanoscale*, is associated with the aggregation and swelling of clay particles (in particular, smectite clay minerals) over distances of tens of nanometers.

Mesoscale phenomena that influence permeability are primarily mechanical and include, for example, the ability of contacts between large grains to prevent the compaction of the clay matrix. Nanoscale phenomena that influence permeability tend to be chemomechanical in nature, because they involve strong impacts of aqueous chemistry on clay swelling. The second length scale remains much less well characterized than the first, because of the inherent challenges associated with the study of strongly coupled nanoscale phenomena.

Advanced models of the nanoscale properties of fine-grained media rely predominantly on the Derjaguin–Landau–Verwey–Overbeek (DLVO) theory, a mean field theory of colloidal interactions that accurately predicts clay swelling in a narrow range of conditions (low salinity, low compaction, Na^+ counterion). An important feature of clay swelling that is not predicted by these models is the coexistence, in most conditions of aqueous chemistry and dry bulk density, of two types of pores between parallel smectite particles: mesopores with a pore width of >3 nm that are controlled by long-range interactions (the *osmotic swelling* regime) and nanopores with a pore width <1 nm that are controlled by short-range interactions (the *crystalline swelling* regime). Nanogeochemical characterization and simulation techniques, including coarse-grained and all-atom molecular dynamics simulations, hold significant promise for the development of advanced constitutive relations that predict this coexistence and its dependence on aqueous chemistry.

1. INTRODUCTION

A core requirement for the implementation of carbon capture and storage (CCS) as a viable CO_2 mitigation technology is the identification of geologic formations that can securely trap supercritical CO_2 for millennia. Of outsized importance in this trapping are the primary seals or caprocks: low-permeability rock formations that overlie storage reservoirs.[1] At existing CCS sites, these seals consist predominantly of fine-grained sedimentary rocks, such as shale or mudstone, the low permeability of which is well established.[2] Predictions of long-term storage security, however, require *predictive models* of the sensitivity of permeability to geomechanical and geochemical alteration including in the presence of fractures and

faults.[3−5] The quality of these models inherently depends on their ability to reflect fundamental controls on fluid flow.

What fundamental features, then, control the permeability of fine-grained sedimentary rocks? The answer remains elusive[6] despite its long-standing importance in groundwater hydrology,[7] basin modeling,[8] petroleum geology,[9] and radioactive waste management[10] as well as, in the case of unconsolidated porous media, in soil science.[11]

The absence of a comprehensive answer is illustrated by the coexistence of three major semiempirical approaches. The first

approach derives from a very simple conceptual model of porous rock as a bundle of capillary tubes of equal radius. On this model, hydraulic permeability, k (m^2), follows the relation[11,12]

$$k = (1/b)R_h{}^2(\phi/\tau^2) \qquad (1)$$

where ϕ, τ, and R_h are the porosity, tortuosity, and hydraulic radius of the porous medium (ratio of pore volume to pore surface area) and $b \approx 2-4$ is a pore shape factor. Variants of eq 1 obtained by expressing R_h as a function of solid specific surface area, a_s, or average grain radius, r_g, or applying the simplifying assumption $\phi/\tau^2 \approx \phi^m$ (where $m = 1.5-2.0$ for pure sand) or both include the well-known Kozeny–Carman relation:[11,13]

$$k = \phi^3/[b\tau^2 a_s(1 - \phi)^2] \qquad (2)$$

and the Revil–Cathles relation:[12]

$$k = r_g{}^2\phi^{3m}/3 \qquad (3)$$

A simplification of eqs 1–3 widely used in groundwater hydrology expresses permeability as having a power-law dependence on porosity:[5]

$$k = k_0\phi^n \qquad (4)$$

where $n \approx 3-15$. A notable variant attempts to reconcile the nonunimodal pore-size distribution of most fine-grained sedimentary rocks[14,15] with the conceptual model used to derive eq 1 by replacing ϕ in eqs 1–4 with $(\phi - \phi_c)$,[16,17] where ϕ_c can be viewed as a critical percolation porosity[16] ($\phi_c = 0.02-0.09$ for overlapping sphere packs[18] and sandstone).[19]

The second approach, sometimes applied in basin modeling and petroleum geology, consists of treating clay content as a key factor controlling the permeability of sedimentary rocks.[9,20–23] Several studies have noted that based on an ideal packing model, the porosity of fine-grained sedimentary rocks should display a minimum at a clay volume (or, almost equivalently, mass) fraction $X_{clay} \approx 1/3$.[12,20,22] Such theoretical packing models have support in laboratory experiments investigating confined sand–clay mixtures under stress[20] as well as field wireline logging studies,[24] where a system transition in the elastic properties is observed at roughly $X_{clay} \approx 1/3$. Revil and Cathles[12] combined the ideal packing model with eq 3 to obtain a model with a permeability minimum at $X_{clay} \approx 1/3$:

$$k = k_S[1 - S_v(1 - \phi_c)/\phi_S]^{3m} \quad \text{if } S_v < \phi_S$$
$$k = k_C(S_v)^{mS} \qquad\qquad\quad\; \text{if } S_v > \phi_S \qquad (5)$$

where k_i, ϕ_i, and m_i are the permeability, porosity, and cementation factors of pure sand and clay ($i = \text{S}$ or C, respectively), m is an effective cementation factor for shaly sand, and S_v is the volume fraction of the porous medium occupied by the microporous clay matrix.

In a related illustration of the importance of clay content, reconstructions of the distribution of hydrocarbons in subsurface reservoirs have shown that the permeability of faults intersecting fine-grained rock formations is controlled by the clay content of the fault-filling material, as quantified by proxies such as the shale gouge ratio (SGR), through parametric relations such as[9]

$$\log k = \log k_0 - 4 \times \text{SGR} - 0.25 \times \log(D)$$
$$\times (1 - \text{SGR})^5 \qquad (6)$$

or[25]

$$\log k = \log k_0 - 3.47 \times \log(\text{SGR}) \qquad (7)$$

where D is the fault displacement in meters. Similarly, parametric models of marine mudstone permeability indicate that the use of clay content (in addition to porosity) as a model parameter decreases the uncertainty of predicted k values by roughly 2 orders of magnitude.[23] The fault and mudstone permeability models noted above display a strong dependence on clay content, but no evidence of a critical threshold at $X_{clay} \approx 1/3$.

The third approach, well established in soil science, follows from the observation that the permeability of fine-grained soils can be highly sensitive to the fraction of swelling (smectite) clay minerals ($X_{smectite}$), the salinity of the pore fluid (C_0), and the fraction of clay negative surface charge balanced by adsorbed sodium (E_{Na}).[13,26] A representative parametric model of this effect is the McNeal relation:[27–29]

$$k = k_0[1 - cf^n] \qquad (8)$$

where c and n are soil-specific parameters and f is a function that increases with E_{Na} and $X_{smectite}$ and decreases with C_0 in a manner that reflects the extensive swelling and dispersion of Na-exchanged smectite at $C_0 < 300$ mol$_c$ m^3.[30] Predictive understanding of this effect remains limited as illustrated by the soil-specific nature of c, n, and f and by the evidence that permeability is sensitive to salinity even in the case of clay minerals other than smectite or exchangeable cations other than sodium.[13,21,26,31] In the case of fine-grained sedimentary rocks, fluid chemistry also influences permeability, but insufficient data exist to establish the validity of eq 8.[6,32]

Collectively, the models summarized above strongly suggest that the permeability of fine-grained sedimentary rocks is a function of at least five parameters (ϕ, X_{clay}, $X_{smectite}$, C_0, E_{Na}). Multiple parametric relations have been proposed with different underlying mathematical forms, but none accounts for all relevant parameters. In addition, the relevance of the models described above in the presence of faults or fractures is not well established.[9] In sections 2 and 3, we summarize recent insights into core- and nanoscale controls on the microstructure of fine-grained porous media, and we discuss implications for the development of advanced permeability models.

2. THE CORE SCALE VIEW: MINERALOGICAL CONTROLS ON THE COMPACTION OF THE CLAY MATRIX

A key challenge in efforts to construct models of the permeability of fine-grained sedimentary rocks is the relative scarcity of experimental data in relation to the parameter space to be explored (porosity, mineralogy, pore water chemistry). This scarcity reflects experimental challenges associated with the study of fine-grained rocks, particularly their lack of mechanical strength, sensitivity to alteration by mechanical unloading, drying, and oxidation, nanometer-scale pore size (to which standard microstructural characterization techniques are poorly adapted), and permeability values so low that measurements can be highly sensitive to minute artifacts.[14,32,33]

Despite the challenges outlined above, sufficient experimental data have emerged over the last two decades to draw

preliminary inferences regarding the impacts of porosity and mineralogy on permeability. A recent compilation of core scale measurements of the permeability of intact rocks[1,2,20] shows that X_{clay} is a key parameter controlling the permeability of sedimentary rocks, in agreement with eqs 5−7 (Figure 1).
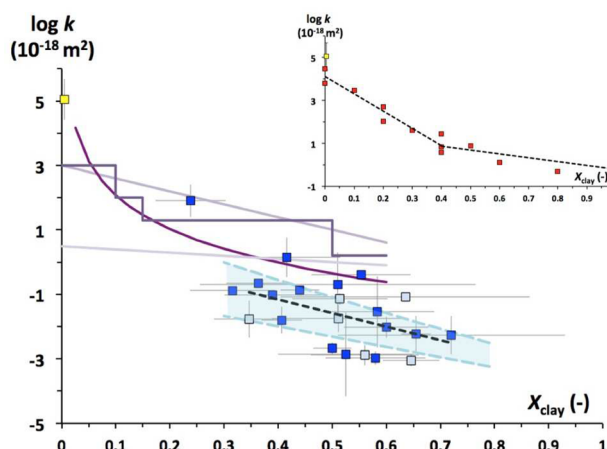

Figure 1. Core scale permeability of well characterized shale and mudstone formations (blue squares) and of pure sandstone (yellow square) as compiled by Bourg.[2] Light blue squares are rocks for which $X_{smectite}$ was reported and was larger than 0.15. The dashed black line is a linear regression of permeability data for rocks with $X_{clay} > 1/3$. The shaded blue region is the mudstone permeability model of Yang and Aplin[23] with ϕ = 0.15 to 0.3. The purple lines are regional scale reconstructions of fault permeability based on known hydrocarbon distributions in different sedimentary basins[9,25] plotted under the assumption that SGR is a reasonable proxy for X_{clay}. The inset shows permeability results obtained with compacted quartz−kaolinite mixtures.[22] Permeability values are either normal to bedding (blue squares, shaded blue region) or parallel to shearing (red squares, purples lines).

Variations in X_{clay} result in up to 8 orders of magnitude differences in rock permeability. The permeability of intact sedimentary rocks is 2 orders of magnitude smaller than that of faults[9,25] and synthetic quartz−kaolinite mixtures.[22] Roughly one-quarter to one-half of this difference is attributable to the known permeability anisotropy of fine-grained rocks (the k values in Figure 1 are normal to bedding for intact rocks, but parallel to shearing for faults and synthetic quartz−kaolinite mixtures).

The results compiled in Figure 1 suggest that the regional scale permeability of faults is broadly analogous to the core scale permeability of intact rock of same mineralogy. This finding is consistent with permeability and X-ray computed tomography (CT) studies of fractured rock cores demonstrating that clay-rich rocks readily self-seal, at least in some conditions, through clay aggregation and clogging[34] or through ductile deformation[35] (Figure 2).

The permeability data in Figure 1 further indicate that the expected transition between intergranular contacts and clay-supported geometries at $X_{clay} \approx 1/3$ (Figure 3a) has only a mild impact on permeability. In particular, it is not associated with a permeability minimum as predicted by eq 5. This behavior contrasts with the existence of a clear threshold at $X_{clay} \approx 1/3$ in the mechanical properties of fine-grained rocks [elastic properties,[20,24] mechanics of fracture slip,[36] mechanical strength (Figure 3b)].[3] Overall, the data suggest that the mesoscale (~10 μm scale) structure of fine-grained rocks exerts

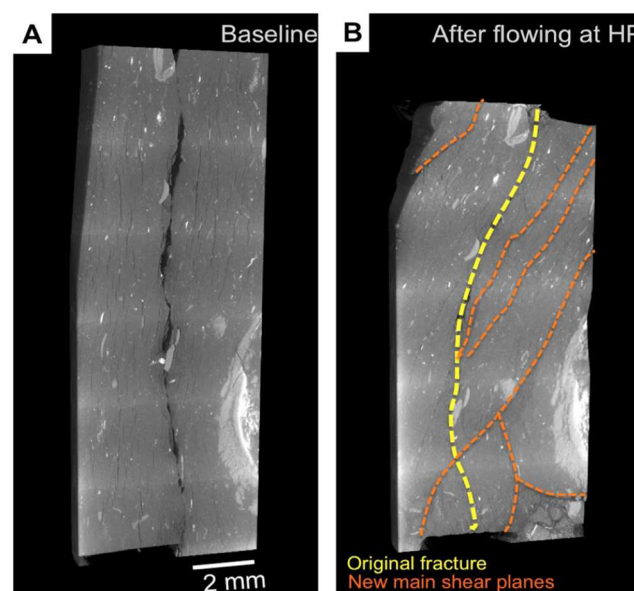**Figure 2.** Evolution of a fracture in clay-rich sedimentary rock (Opalinus clay, X_{clay} = 0.60 ± 0.08) while under stress as imaged by X-ray CT. Panels A and B show ductile evolution of an initially open fracture (A) and closure after flow of water with dissolved CO_2 (B), Images were obtained under in situ conditions of fluid pressure (9.7 MPa) and confining pressure (11.0 MPa). The results are consistent with the low strength of clay-rich rocks (Figure 3b). Reproduced with permission from Marco Voltolini.
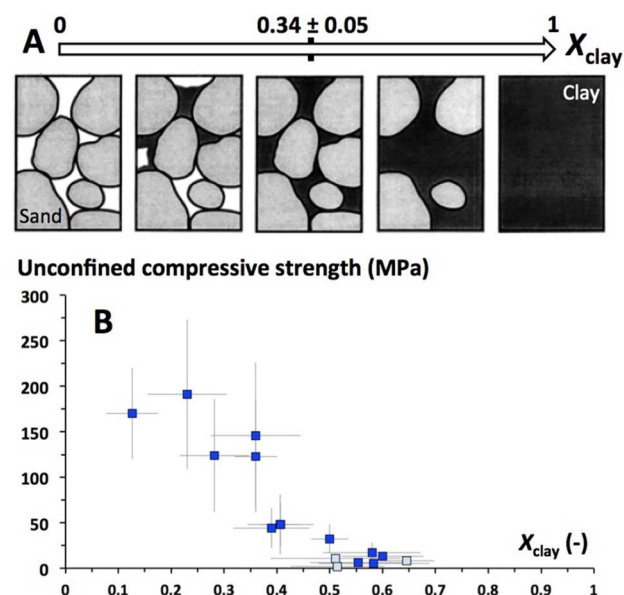

Figure 3. (A) Conceptual model of the mesoscale structure of sedimentary rocks as an assemblage of large grains (gray), macropores (white), and fine-grained clay matrix (black).[2,12,20,22] Clay mineral mass fraction (X_{clay}) increases from left to right. Simple geometric calculations indicate that the clay matrix is the load bearing phase if $X_{clay} \geq 0.34 \pm 0.10$.[2] (B) Core scale measurements of unconfined compressive strength as a function of X_{clay} from the same compilation as in Figure 1.[2]

a strong influence on their mechanical properties, but less influence on the permeability of intact rock samples.

Porosity plays an important secondary role in determining the permeability of fine-grained sedimentary rocks. However,

permeability does not exhibit a simple power-law dependence on ϕ, as implied by eqs 1−4, or a critical porosity ϕ_c below which $k = 0$ (Figure 4).[1,2,23] Instead, k becomes essentially
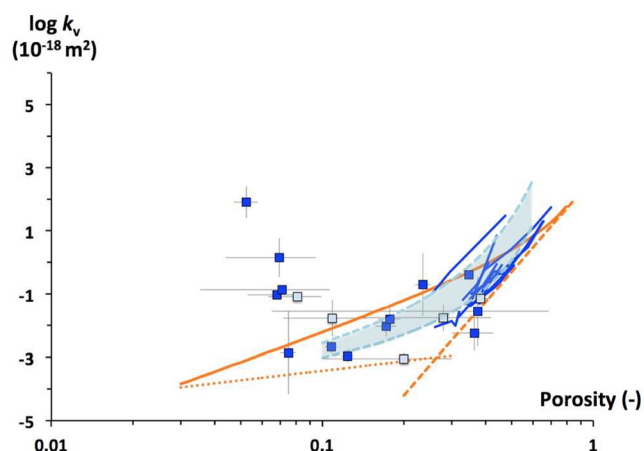

Figure 4. Same data as in Figure 1 plotted as a function of total porosity.[1,2] Dark blue lines are a representative selection of normally consolidated clay-rich sediments compacted to a range of ϕ values using a standard oedometric test.[1] The shaded blue region represents the mudstone permeability model of Yang and Aplin[23] with $X_{clay} = 0.4$ to 0.6. The solid and dashed orange lines show the permeability of pure Illite predicted with eq 2 (with a particle thickness of 20 phyllosilicate layers) and eq 3 (with $r_g = 21.6$ nm and $m = 3.28$).[12] The dotted orange line reflects the water flux that would occur by pressure-driven molecular diffusion, a plausible lower boundary on k_v.[1]

independent of porosity at $\phi < 0.2$. This behavior has been attributed to the bimodal (or more complex) pore-size distribution of fine-grained rocks, where larger pores are preferentially eliminated by compaction.[33] This behavior contrasts with observed porosity−permeability relationships in cemented sandstones.[37]

3. THE NANOSCALE VIEW: CHEMICAL CONTROLS ON THE MECHANICS OF CLAY SWELLING

The results presented above suggest that the permeability of water-saturated clay-rich rocks ($X_{clay} > 1/3$) is controlled by the permeability of the clay matrix[12,20] or, more precisely, by the size and connectivity of the largest pores in the clay matrix.[14] An understanding of these pores is emerging thanks to the use of small-angle neutron scattering (SANS) and focused ion beam scanning or transmission electron microscopy (FIB-SEM/TEM) (Figure 5).[6,14,15] In clay-rich rocks, these techniques reveal median pore diameters on the order of 1 to 10 nm, with few connected pores larger than 10 nm.[14,38] Exposure to solutions with different chemistries significantly modifies the population and connectivity of nanopores and mesopores, perhaps reflecting the aqueous chemistry dependence of clay swelling.[38] The sensitivity of microstructure to stress conditions is expected to be significant but remains sparsely studied.[14,15,33,38]

A more detailed understanding of clay microstructure, permeability, and related properties as a function of compaction and pore water chemistry exists in the case of pure clay minerals and clay−sand mixtures.[26,39−41] These media constitute reasonable proxies for the clay matrix, at least in some cases, as indicated by the similar permeability trends of sedimentary rocks and kaolinite−quartz mixtures (Figure 1) and by the
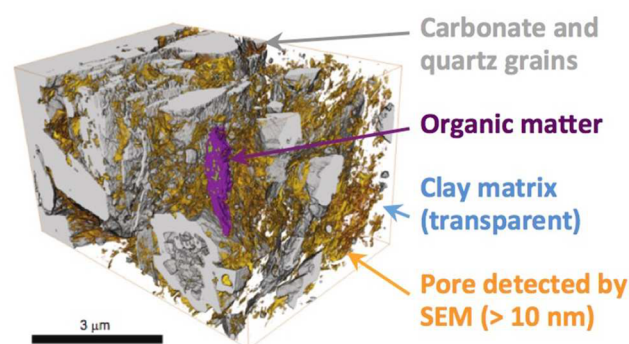

Figure 5. FIB-SEM reconstruction of the microstructure of a clay-rich rock (Opalinus clay, $X_{clay} = 0.60 \pm 0.08$). About 80% of the pore space is located in pores smaller than the 10 nm resolution of the image; the remainder, shown in gold color, consists of mesopores distributed within the clay matrix.[14] The image is consistent with the clay matrix being the phase that controls the permeability of clay-rich rocks. Adapted with permission from ref 14. Copyright 2013 Elsevier.

qualitative consistency between water and solute diffusion coefficients in clay-rich rocks and in compacted water-saturated smectite.[42] Electron microscopy images indicate that fluid flow in intact clay-rich rocks is controlled by pore throats with the same width as the largest pores in compacted smectite.[14,40] This analogy between pure clay and fine-grained rocks is consistent with the effective degree of compaction of the clay matrix being a key parameter controlling swelling pressure,[43] water and solute diffusion,[42] and permeability[12,20] in fine grained porous media.

The predominant conceptual model of the microstructure of compacted, water-saturated clay is one in which individual phyllosilicate layers (1 nm thick, 50−2000 nm in diameter) are arranged into stacks (up to ∼100 layers per stack) referred to as tactoids, domains, or quasicrystals.[26,39,43−46] Colloidal interactions, characterized extensively in the case of smectite clay using X-ray diffraction (XRD) experiments, give rise to *crystalline swelling* states with interparticle distances of 0.3, 0.6, and 0.9 nm (where the interlayers are intercalated with one, two, or three monolayers of water molecules) and an *osmotic swelling* regime with interparticle distances of 2.5 to >14 nm.[30,39−41,47] The resulting microstructure contains three types of pores: "crystalline" nanopores, "osmotic" mesopores, and, in some cases, macropores (Figure 6). The relative stability of the different swelling states, and the value of the preferred interparticle distance in the osmotic swelling regime, are functions of salinity, the identity of the exchangeable cations, the degree of compaction, the number of clay layers per stack, and the hydration history of the sample.[30,40,44,47,48]

A more detailed understanding of clay aggregation structure has proved challenging to establish, because many techniques either provide indirect evidence (as in the case of rheology, coagulation kinetics, or light transmission measurements)[49] or require drying the clay (as in the case of TEM).[21] In the past decade, advances in small-angle X-ray scattering (SAXS), transmission X-ray microscopy (TXM), and cryogenic TEM (cryo-TEM) methodologies have provided new insight into the microstructure of smectite clay in aqueous suspension[45,48,50−52] and in compacted samples.[41] For example, these studies have shown that the basal spacing of the osmotic hydrate decreases with the number of particles per stack[48,52] and that clay aggregation by edge-to-face interactions is much less prevalent than previously hypothesized.[45,48,50,52] The picture that
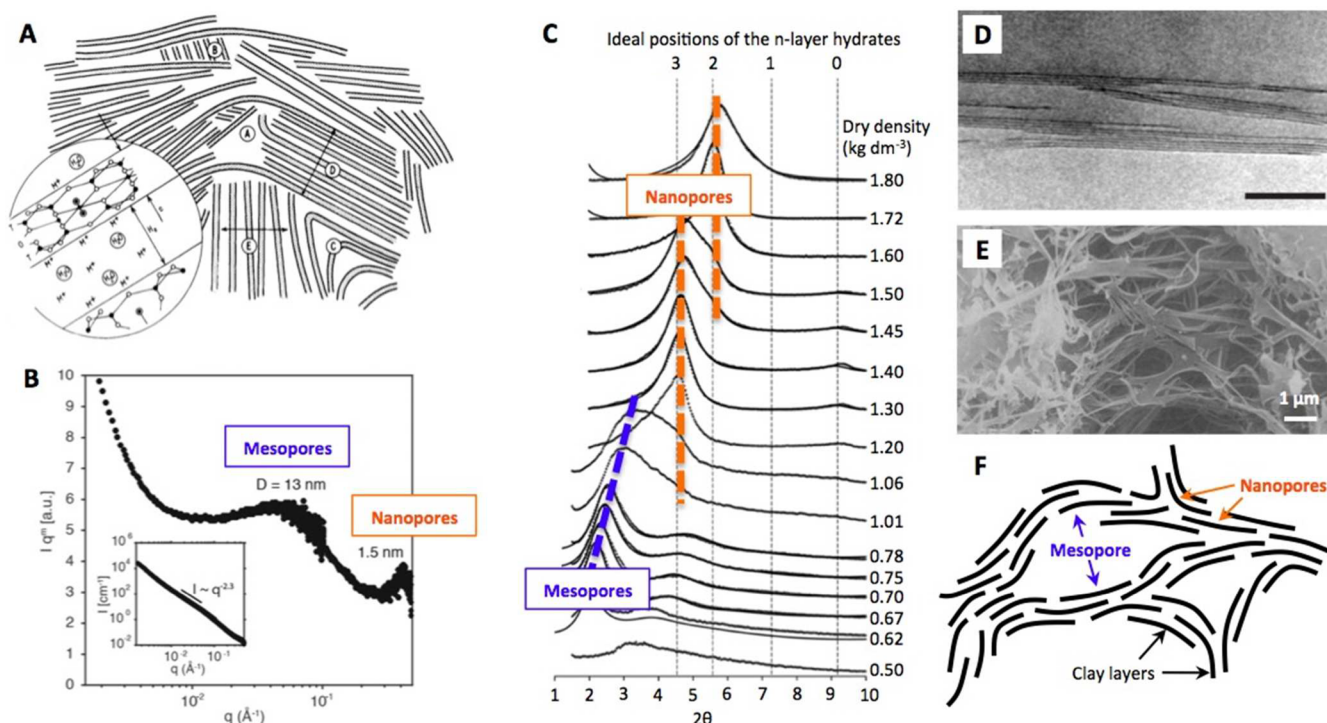
Figure 6. Microstructure of compacted smectite clay. (A) Conceptual model of the microstructure of smectite clay hydrated with humid air (only crystalline swelling is present).[39] (B) SAXS data for K-smectite particles suspended in a 0.1 M KCl solution[52] showing the coexistence of nanopores and mesopores (with basal spacings of 1.5 and 13 nm). (C) XRD data for Na-smectite compacted to a range of dry bulk densities and hydrated with pure liquid water.[40] (D) cryo-TEM image of smectite particles in bulk liquid water revealing no evidence of edge-to-face aggregation (scale bar is 50 nm). (E) TEM image of a sandstone with 5% smectite content indicating the existence of pore-bridging smectite strands too extensive to consist of individual smectite layers.[21] (F) Conceptual model of the microstructure of smectite clay hydrated with liquid water showing partly overlapping layers and a phase separation between mesopores and nanopores. Panel A reproduced with permission from ref 39. Copyright 1979 The Clay Minerals Society. Panels B and D reproduced with permission from ref 52. Copyright 2016 American Chemical Society. Panel C adapted with permission from ref 40. Copyright 2012 Elsevier. Panel E reproduced with permission from ref 21. Copyright 1998 The Clay Minerals Society.

emerges is one in which stacks of partly overlapping particles organize into three-dimensional structures with internal nano- and mesoporosity controlled by the type of exchangeable cation[45] and coexisting in a manner analogous to a phase separation.[48,51] Macropores are absent in compacted Na-smectite hydrated with low-salinity water[40,41] and likely exist only in situations where swelling capacity is insufficient to fill the entire available space.[21]

Efforts to account for the microstructure of the clay matrix in geochemical and geomechanical simulations have led to the development of so-called *dual structure models* in which the pore space is conceptually divided into two compartments (macropores and micropores, with volume fractions ϕ_M and ϕ_m) that exchange fluid and solutes with each other as a function of stress, water saturation, and pore water chemistry.[46,53−57] The micropores as defined in these models include both the meso- and nanopores defined above. Permeability is modeled as a function of ϕ_M based either on an empirical relation[46] or an assumed geometry of the macropores.[54,55] Models of this type have focused on swelling mechanics,[46,53] ionic transport,[55] and self-diffusion in clayey media[56] and have not been extensively tested against laboratory permeability data or larger scale field studies of transport.

In the dual structure models introduced above, the swelling mechanics of meso- and nanopores are based either on parametric fits to macroscopic scale measurements of clay swelling pressure[46] or on the Derjaguin−Landau−Verwey−Overbeek (DLVO) theory,[26,43,53−55] a mean field theory of long-range colloidal interactions (London dispersion, electrostatic repulsion). The DLVO-based models, though predominantly used, are strictly valid only in conditions where osmotic swelling predominates (i.e., pure Na-smectite at ionic strengths below 0.2 M and low degrees of compaction) because they inherently do not account for short-range attractive interactions that control the stability of the crystalline hydrates.[26,30,40,44,51,52] Efforts to refine these models have been significant (for example, by accounting for surface complexes[58] and surface hydration forces[43,54] and more accurately quantifying the London dispersion forces)[52] but have not yet addressed the failure of DLVO theory to predict the coexistence of crystalline and osmotic hydrates.[30,40,48,52] A promising approach to remedy this weakness may be to treat the crystalline swelling states as distinct thermodynamic phases where the partial specific free energy of water is strongly modulated by short-range interactions.[44,57]

Nanoscale simulations of clay aggregation at the scale of individual layers have the potential to support the development of dual structure models by providing insight into the microstructure of clayey media (Figure 6). Efforts in this direction have modeled either pairs of clay particles in liquid water [using molecular dynamics (MD) or Monte Carlo (MC) simulations with an all-atom[59,60] or implicit solvent][51,61] or assemblages of hundreds of clay particles (using coarse-grained simulations with interparticle interaction potentials derived from all-atoms MD simulations[59] or DLVO theory).[50,62−65]
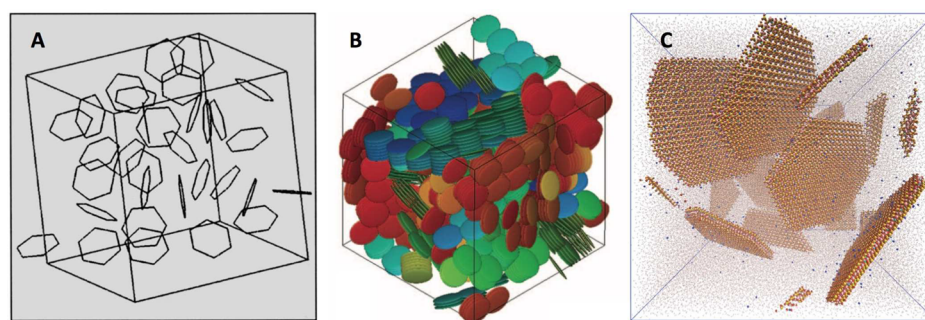
Figure 7. Nanoscale simulations of clay aggregation at the scale of individual layers. (A) Coarse-grained simulation with an interaction potential based on DLVO theory.[63] (B) Coarse-grained simulation with an interaction potential based on all-atom MD simulations of two smectite particles.[59] (C) All-atom MD simulation of ten Na-smectite nanoparticles (10 nm in diameter) in liquid water. Panel A reproduced with permission from ref 63. Copyright 2000 The American Institute of Physics. Panel B reproduced with permission from ref 59. Copyright 2000 The American Institute of Physics.

Most studies to date, with a few exceptions,[51,60,61] have focused on the swelling mechanics of Na-smectite in pure liquid water.

A key challenge associated with the coarse-grained models outlined above is the difficulty of developing interparticle interaction models that accurately reflect both long- and short-range interactions. Most of the models developed to date assume that particle—particle interactions are repulsive at all distances, and none of them predicts the coexistence of osmotic and crystalline hydrates.[61−65] Several coarse-grained models have reported reasonable agreement with experimental data on the swelling pressure of Na-smectite in pure water,[59,65] but none has yet been validated against data on the detailed pore-size distribution of compacted smectite[40,41] or against properties that are particularly sensitive to pore-size distribution, such as anion exclusion or permeability.

The all-atom simulations studies outlined above, though inherently more fundamental than the coarse-grained models, involve significant challenges, as indicated by the existence of only two all-atom MD simulation studies probing the free energy of interaction of smectite particles for a relatively narrow range of configurations and aqueous chemistries.[59,60] Future developments in this area are likely, as shown by recent advances in the simulation of stable, fully flexible clay edge surfaces,[66,67] by successful validations of existing interatomic potential models against experimental data on the structure, dynamics, and energetics of water and ions on clay basal surfaces,[68,69] and by sustained advances in high-performance computing resources that have increased the size of tractable systems from ∼10^2 nm³[59,60] to ∼10^4 nm³ over the last half-decade, as required to model systems containing tens of smectite nanoparticles in liquid water (Figure 7c).

4. CONCLUSIONS

The permeability of fine-grained sedimentary rocks depends significantly on porosity, mineralogy, and pore water chemistry. The development of advanced permeability models requires new understanding of the mesoscale mechanics of sedimentary rocks, the nanoscale impacts of aqueous chemistry and dry density on the microstructure and permeability of the clay matrix, and the links between both scales. The second question is particularly challenging, because it involves strong nanoscale chemomechanical couplings. Advances in nanogeochemical characterization and simulation techniques (including synchrotron X-rays and neutrons, high-resolution electron microscopy, and high-performance computing) have the potential to yield new constitutive models of the microstructure, mechanics, and permeability of the clay matrix and its dependence on aqueous chemistry and compaction that may, when combined with existing mesoscale simulation methodologies,[70,71] enable significant advances in predicting the permeability of fine-grained rocks.

■ AUTHOR INFORMATION

Corresponding Author

*E-mail: bourg@princeton.edu.

ORCID ⓘ

Ian C. Bourg: 0000-0002-5265-7229

Notes

The authors declare no competing financial interest.

Biographies

Ian Bourg was born in Massachusetts in 1976. He received in B.Eng. from the National Institute of Applied Sciences in Toulouse in 1999 and his Ph.D. from the University of California at Berkeley in 2004. He was a postdoctoral fellow at the University of Chicago and a Research Scientist at the Lawrence Berkeley National Laboratory before joining the faculty at Princeton University. He and his group study the impacts of interfacial water on the properties of natural and engineered systems.

Jonathan Ajo-Franklin was born in St. Louis, Missouri, in 1975. He received his B.A. in Computer Science and History from Rice University in 1998 and his M.S. (2003) and Ph.D (2005) from Stanford University in Geophysics. He was a postdoctoral fellow at MIT before joining Lawrence Berkeley National Laboratory as a Research Scientist. He is presently a Staff Scientist and the Department Head of Geophysics at LBNL. He and his group study geophysical approaches for monitoring rock and soil transformations relevant to energy and environmental applications at a range of scales.

are grateful to Marco Voltolini for use of the images shown in Figure 4, which were acquired at the Advanced Light Source, Beamline 8.3.2, supported by the Office of Science, Office of Basic Energy Sciences, of the U.S. DOE (contract DE-AC02-05CH11231).

■ REFERENCES

(1) Bourg, I. C.; Beckingham, L. E.; DePaolo, D. J. The Nanoscale Basis of CO_2 Trapping for Geologic Storage. *Environ. Sci. Technol.* **2015**, *49*, 10265−10284.

(2) Bourg, I. C. Sealing Shales versus Brittle Shales: A Sharp Threshold in the Material Properties and Energy Technology Uses of Fine-Grained Sedimentary Rocks. *Environ. Sci. Technol. Lett.* **2015**, *2*, 255−259.

(3) Zoback, M. D.; Gorelick, S. M. Earthquake Triggering and Large-Scale Geologic Storage of Carbon Dioxide. *Proc. Natl. Acad. Sci. U. S. A.* **2012**, *109*, 10164−10168.

(4) Fitts, J. P.; Peters, C. A. Caprock Fracture Dissolution and CO_2 Leakage. *Rev. Mineral. Geochem.* **2013**, *77*, 459−479.

(5) Rinaldi, A. P.; Jeanne, P.; Rutqvist, J.; Cappa, F.; Guglielmi, Y. Effects of Fault-Zone Architecture on Earthquake Magnitude and Gas Leakage Related to CO_2 Injection in a Multi-Layered Sedimentary System. *Greenhouse Gases: Sci. Technol.* **2014**, *4*, 99−120.

(6) Ilgen, A. G.; Heath, J. E.; Akkutlu, I. Y.; Bryndzia, L. T.; Cole, D. R.; Kharaka, Y. K.; Kneafsey, T. J.; Milliken, K. L.; Pyrak-Nolte, L. J.; Suarez-Rivera, R. Shales at All Scales: Exploring Coupled Processes in Mudrocks. *Earth-Sci. Rev.* **2017**, *166*, 132−152.

(7) Meyer, J. R.; Parker, B. L.; Cherry, J. A. Characteristics of High Resolution Hydraulic Head Profiles and Vertical Gradients in Fractured Sedimentary Rocks. *J. Hydrol.* **2014**, *517*, 493−507.

(8) Cosgrove, J. W. Hydraulic Fracturing during the Formation and Deformation of a Basin: A Factor in the Dewatering of Low-Permeability Sediments. *AAPG Bull.* **2001**, *85*, 737−748.

(9) Manzocchi, T.; Childs, C.; Walsh, J. J. Faults and Fault Properties in Hydrocarbon Flow Models. *Geofluids* **2010**, *10*, 94−113.

(10) Mazurek, M.; Alt-Epping, P.; Bath, A.; Gimmi, T.; Waber, H. N.; Buschaert, S.; De Cannière, P.; De Craen, M.; Gautschi, A.; Savoye, S.; Vinsot, A.; Wemaere, I.; Wouters, L. Natural Tracer Profiles across Argillaceous Formations. *Appl. Geochem.* **2011**, *26*, 1035−1064.

(11) Assouline, S.; Or, D. Conceptual and Parametric Representation of Soil Hydraulic Properties: A Review. *Vadose Zone J.* **2013**, *12*.

(12) Revil, A.; Cathles, L. M., III Permeability of Shaly Sands. *Water Resour. Res.* **1999**, *35*, 651−662.

(13) Shainberg, I.; Letey, J. Response of Soils to Sodic and Saline Conditions. *Hilgardia* **1984**, *52*, 1−57.

(14) Keller, L. M.; Schuetz, P.; Erni, R.; Rossell, M. D.; Lucas, F.; Gasser, P.; Holzer, L. Characterization of Multi-Scale Microstructural Features in Opalinus Clay. *Microporous Mesoporous Mater.* **2013**, *170*, 83−94.

(15) Swift, A. M.; Anovitz, L. M.; Sheets, J. M.; Cole, D. R.; Welch, S. A.; Rother, G. Relationship between Mineralogy and Porosity in Seals Relevant to Geologic CO_2 Sequestration. *Environ. Geosci.* **2014**, *21*, 39−57.

(16) Quispe, J. R.; Rozas, R. E.; Toledo, P. G. Permeability−porosity Relationship from a Geometrical Model of Shrinking and Lattice Boltzmann and Monte Carlo Simulations of Flow in Two-Dimensional Pore Networks. *Chem. Eng. J.* **2005**, *111*, 225−236.

(17) Ahuja, L. R.; Cassel, D. K.; Bruce, R. R.; Barnes, B. B. Evaluation of Spatial Distribution of Hydraulic Conductivity Using Effective Porosity Data. *Soil Sci.* **1989**, *148*, 404−411.

(18) Martys, N. S.; Torquato, S.; Bentz, D. P. Universal Scaling of Fluid Permeability for Sphere Packings. *Phys. Rev. E* **1994**, *50*, 403−408.

(19) Gomez, C. T.; Dvorkin, J.; Vanorio, T. Laboratory Mesurements of Porosity, Permeability, Resistivity, and Velocity on Fontainebleau Sandstones. *Geophysics* **2010**, *75*, E191−E204.

(20) Marion, D.; Nur, A.; Yin, H.; Han, D. Compressional Velocity and Porosity in Sand-Clay Mixtures. *Geophysics* **1992**, *57*, 554−563.

(21) Nadeau, P. H. An Experimental Study of the Effects of Diagenetic Clay Minerals on Reservoir Sands. *Clays Clay Miner.* **1998**, *46*, 18−26.

(22) Crawford, B. R.; Faulkner, D. R.; Rutter, E. H. Strength, Porosity, and Permeability Development during Hydrostatic and Shear Loading of Synthetic Quartz-Clay Fault Gouge. *J. Geophys. Res.* **2008**, *113*, B03207.

(23) Yang, Y.; Aplin, A. C. A Permeability−porosity Relationship for Mudstones. *Mar. Pet. Geol.* **2010**, *27*, 1692−1697.

(24) Herron, S. L.; Herron, M. M.; Plumb, R. A. Identification of Clay-Supported and Framework-Supported Domains From Geochemical and Geophysical Well Log Data. SPE Annual Technical Conference and Exhibition, 1992, SPE Paper 24726, DOI: 10.2118/24726-MS.

(25) Jolley, S. J.; Dijk, H.; Lamens, J. H.; Fisher, Q. J.; Manzocchi, T.; Eikmans, H.; Huang, Y. Faulting and Fault Sealing in Production Simulation Models: Brent Province, Northern North Sea. *Pet. Geosci.* **2007**, *13*, 321−340.

(26) Quirk, J. P. Soil Permeability in Relation to Sodicity and Salinity. *Philos. Trans. R. Soc., A* **1986**, *316*, 297−317.

(27) McNeal, B. L.; Layfield, D. A.; Norvell, W. A.; Rhoades, J. D. Factors Influencing Hydraulic Conductivity of Soil in the Presence of Mixed-Salt Solutions. *Soil Sci. Soc. Am. Proc.* **1968**, *32*, 187−190.

(28) van der Zee, S. E. A. T. M.; Shah, S. H. H.; Vervoort, R. W. Root Zone Salinity and Sodicity under Seasonal Rainfall due to Feedback of Decreasing Hydraulic Conductivity. *Water Resour. Res.* **2014**, *50*, 9432−9446.

(29) Mau, Y.; Porporato, A. Optimal Control Solutions to Sodic Soil Reclamation. *Adv. Water Resour.* **2016**, *91*, 37−45.

(30) Norrish, K. Manner of Swelling of Montmorillonite. *Nature* **1954**, *173*, 256−257.

(31) Mesri, G.; Olson, R. E. Mechanisms Controlling the Permeability of Clays. *Clays Clay Miner.* **1971**, *19*, 151−158.

(32) Kwon, O.; Herbert, B. E.; Kronenberg, A. K. Permeability of Illite-Bearing Shale: 2. Influence of Fluid Chemistry on Flow and Functionally Connected Pores. *J. Geophys. Res.* **2004**, *109*, B10206.

(33) Best, M. E.; Katsube, T. J. Shale Permeability and Its Significance in Hydrocarbon Exploration. *Leading Edge* **1995**, *14*, 165−170.

(34) Noiriel, C.; Madé, B.; Gouze, P. Impact of Coating Development on the Hydraulic and Transport Properties in Argillaceous Limestone Fracture. *Water Resour. Res.* **2007**, *43*, W09406.

(35) Gutierrez, M.; Øino, L. E.; Nygård, R. Stress-Dependent Permeability of a de-Mineralised Fracture in Shale. *Mar. Pet. Geol.* **2000**, *17*, 895−907.

(36) Kohli, A. H.; Zoback, M. D. Frictional Properties of Shale Reservoir Rocks. *J. Geophys. Res.* **2013**, *118*, 5109−5125.

(37) Grude, S.; Dvorkin, J.; Landrø, M. Permeability Variation with Porosity, Pore Space Geometry, and Cement Type: A Case History from the Snøhvit Field, the Barents Sea. *Geophysics* **2015**, *80*, D43−D49.

(38) Mouzakis, K. M.; Navarre-Sitchler, A. K.; Rother, G.; Bañuelos, J. L.; Wang, X.; Kaszuba, J. P.; Heath, J. E.; Miller, Q. R. S.; Alvarado, V.; McCray, J. E. Experimental Study of Porosity Changes in Shale Caprocks Exposed to CO_2-Saturated Brines I: Evolution of Mineralogy, Pore Connectivity, Pore Size Distribution, and Surface Area. *Environ. Eng. Sci.* **2016**, *33*, 725−735.

(39) Cebula, D. J.; Thomas, R. K.; Middleton, S.; Ottewill, R. H.; White, J. W. Neutron Diffraction from Clay-Water Systems. *Clays Clay Miner.* **1979**, *27*, 39−52.

(40) Holmboe, M.; Wold, S.; Jonsson, M. Porosity Investigation of Compacted Bentonite Using XRD Profile Modeling. *J. Contam. Hydrol.* **2012**, *128*, 19−32.

(41) Muurinen, A.; Carlsson, T.; Root, A. Bentonite Pore Distribution Based on SAXS, Chloride Exclusion and NMR Studies. *Clay Miner.* **2013**, *48*, 251−266.

(42) Bourg, I. C.; Tournassat, C. Self-Diffusion of Water and Ions in Clay Barriers. In *Natural and Engineered Clay Barriers*; Elsevier, 2015; pp 189−226.

(43) Liu, L. Prediction of Swelling Pressures of Different Types of Bentonite in Dilute Solutions. *Colloids Surf., A* **2013**, *434*, 303−318.

(44) Laird, D. A.; Shang, C. Relationship between Cation Exchange Selectivity and Crystalline Swelling in Expanding 2:1 Phyllosilicates. *Clays Clay Miner.* **1997**, *45*, 681−689.

(45) Michot, L. J.; Bihannic, I.; Thomas, F.; Lartiges, B. S.; Waldvogel, Y.; Caillet, C.; Thieme, J.; Funari, S. S.; Levitz, P. Coagulation of Na-Montmorillonite by Inorganic Cations at Neutral pH. A Combined Transmission X-Ray Microscopy, Small Angle and Wide Angle X-Ray Scattering Study. *Langmuir* **2013**, *29*, 3500−3510.

(46) Vilarrasa, V.; Rutqvist, J.; Blanco Martin, L.; Birkholzer, J. Use of a Dual-Structure Constitutive Model for Predicting the Long-Term Behavior of an Expansive Clay Buffer in a Nuclear Waste Repository. *Int. J. Geomech.* **2016**, *16*, D4015005.

(47) Wilson, J.; Cuadros, J.; Cressey, G. An in-Situ Time-Resolved XRD-PSD Investigation into Na-Montmorillonite Interlayer and Particle Rearrangement during Dehydration. *Clays Clay Miner.* **2004**, *52*, 180−191.

(48) Gilbert, B.; Comolli, L. R.; Tinnacher, R. M.; Kunz, M.; Banfield, J. F. Formation and Restacking of Disordered Smectite Osmotic Hydrates. *Clays Clay Miner.* **2015**, *63*, 432−442.

(49) Tombácz, E.; Szekeres, M. Colloidal Behavior of Aqueous Montmorillonite Suspensions: The Specific Role of pH in the Presence of Indifferent Electrolytes. *Appl. Clay Sci.* **2004**, *27*, 75−94.

(50) Jönsson, B.; Labbez, C.; Cabane, B. Interaction of Nanometric Clay Platelets. *Langmuir* **2008**, *24*, 11406−11413.

(51) Segad, M.; Jönsson, B.; Åkesson, T.; Cabane, B. Ca/Na Montmorillonite: Structure, Forces and Swelling Properties. *Langmuir* **2010**, *26*, 5782−5790.

(52) Tester, C. C.; Aloni, S.; Gilbert, B.; Banfield, J. F. Short- and Long-Range Attractive Forces That Influence the Structure of Montmorillonite Osmotic Hydrates. *Langmuir* **2016**, *32*, 12039−12046.

(53) Loret, B.; Hueckel, T.; Gajo, A. Chemo-Mechanical Coupling in Saturated Porous Media: Elastic-Plastic Behaviour of Homoionic Expansive Clays. *Int. J. Solids Struct.* **2002**, *39*, 2773−2806.

(54) Tuller, M.; Or, D. Hydraulic Functions for Swelling Soils: Pore Scale Considerations. *J. Hydrol.* **2003**, *272*, 50−71.

(55) Murad, M. A.; Moyne, C. A Dual-Porosity Model for Ionic Solute Transport in Expansive Clays. *Comput. Geosci.* **2008**, *12*, 47−82.

(56) Bourg, I. C.; Sposito, G. Connecting the Molecular Scale to the Continuum Scale for Diffusion Processes in Smectite-Rich Porous Media. *Environ. Sci. Technol.* **2010**, *44*, 2085−2091.

(57) Sedighi, M.; Thomas, H. R. Micro Porosity Evolution in Compacted Swelling Clays — A Chemical Approach. *Appl. Clay Sci.* **2014**, *101*, 608−618.

(58) Gonçalvès, J.; Rousseau-Gueutin, P.; Revil, A. Introducing Interacting Diffuse Layers in TLM Calculations: A Reappraisal of the Influence of the Pore Size on the Swelling Pressure and the Osmotic Efficiency of Compacted Bentonites. *J. Colloid Interface Sci.* **2007**, *316*, 92−99.

(59) Ebrahimi, D.; Whittle, A. J.; Pellenq, R. J.-M. Mesoscale Properties of Clay Aggregates from Potential of Mean Force Representation of Interactions between Nanoplatelets. *J. Chem. Phys.* **2014**, *140*, 154309.

(60) Sun, L.; Hirvi, J. T.; Schatz, T.; Kasa, S.; Pakkanen, T. A. Estimation of Montmorillonite Swelling Pressure: A Molecular Dynamics Approach. *J. Phys. Chem. C* **2015**, *119*, 19863−19868.

(61) Meyer, S.; Levitz, P.; Delville, A. Influence of the Relative Orientation of Two Charged Anisotropic Colloidal Particles on Their Electrostatic Coupling: A (N,V,T) Monte Carlo Study. *J. Phys. Chem. B* **2001**, *105*, 10684−10690.

(62) Dijkstra, M.; Hansen, J.-P.; Madden, P. A. Statistical Model for the Structure and Gelation of Smectite Clay Suspensions. *Phys. Rev. E* **1997**, *55*, 3044−3053.

(63) Kutter, S.; Hansen, J.-P.; Sprik, M.; Boek, E. Structure and Phase Behavior of a Model Clay Dispersion: A Molecular-Dynamics Investigation. *J. Chem. Phys.* **2000**, *112*, 311−322.

(64) Anandarajah, A.; Amarasinghe, P. M. Discrete-Element Study of the Swelling Behaviour of Na-Montmorillonite. *Geotechnique* **2013**, *63*, 674−681.

(65) Bayesteh, H.; Mirghasemi, A. A. Procedure to Detect the Contact of Platy Cohesive Particles in Discrete Element Analysis. *Powder Technol.* **2013**, *244*, 75−84.

(66) Lammers, L. N.; Bourg, I. C.; Okumura, M.; Kolluri, K.; Sposito, G.; Machida, M. Molecular Dynamics Simulations of Cesium Adsorption on Illite Nanoparticles. *J. Colloid Interface Sci.* **2017**, *490*, 608−620.

(67) Kwon, K. D.; Newton, A. G. Structure and Stability of Pyrophyllite Edge Surfaces: Effect of Temperature and Water Chemical Potential. *Geochim. Cosmochim. Acta* **2016**, *190*, 100−114.

(68) Holmboe, M.; Bourg, I. C. Molecular Dynamics Simulations of Water and Sodium Diffusion in Smectite Interlayer Nanopores as a Function of Pore Size and Temperature. *J. Phys. Chem. C* **2014**, *118*, 1001−1013.

(69) Bourg, I. C.; Lee, S. S.; Fenter, P.; Tournassat, C. Stern Layer Structure and Energetics at Mica-Water Interfaces. *J. Phys. Chem. C* **2017**, *121*, 9402−9412.

(70) Mehmani, A.; Prodanović, M. The Effect of Microporosity on Transport Properties in Porous Media. *Adv. Water Resour.* **2014**, *63*, 104−119.

(71) Soulaine, C.; Tchelepi, H. A. Micro-Continuum Approach for Pore-Scale Simulation of Subsurface Processes. *Transp. Porous Media* **2016**, *113*, 431−456.